# Performance Evaluation of SPRINT, A Single Photon Ring Tomograph for Brain Imaging

W. Leslie Rogers, Neal H. Clinthorne, John Stamos, Kenneth F. Koral, Robert Mayans, Glenn F. Knoll, Jack Juni, John W. Keyes, Jr., and Beth A. Harkness

*University of Michigan, Ann Arbor, Michigan*

**SPRINT, a prototype single photon tomograph, has been designed primarily for high-resolution brain imaging in humans with I-123-labeled compounds such as iodoamphetamine, hydroxyiodopropyldiamine (HIPDM), and iodobenzene (IBZ). SPRINT uses a ring of stationary, discrete NaI detectors, and fan-beam sampling is accomplished with a rotating eight-slit aperture ring that acquires a complete projection set in 1/8 revolution. In-plane and cross-plane resolutions are 8mm and 10mm FWHM, respectively, measured on axis. Sensitivity with an 18% energy window is 1000 cprs per μCi/cc for Tc-99m in a 20 cm diameter phantom. A detailed evaluation of system performance has been completed, and preliminary human brain blood flow images have been obtained using HIPDM.**

**J Nucl Med 25: 1013–1018, 1984**

Two I-123 labeled compounds recently described show great promise for measuring regional cerebral blood flow (*1–4*). A third compound has been described as a myelin stain (*5*). These compounds have spurred interest in high-resolution tomographic imaging of the brain. SPRINT, a prototype single photon ring tomograph, is being developed with these applications in mind.

The construction and preliminary specifications of SPRINT have been described (*6*). Briefly, SPRINT is designed with discrete sodium iodide detectors arranged in a fixed ring 70 cm in diameter. A complete set of fan-beam projections for the 20-cm field of view is acquired by means of a rotating lead aperture ring containing eight slits. Converging cross-plane collimation is achieved with lead foil rings sandwiched between tapered styrofoam spacers. Both the aperture ring and collimator may be replaced with other apertures to obtain different imaging properties.

Received Feb. 16, 1984; revision accepted May 14, 1984.

For reprints contact: W. Leslie Rogers, PhD, University of Michigan Medical School, Cyclotron/PET Facility, 3480 Kresge I Box 056, Ann Arbor, MI 48109.

This paper gives detailed measurements of system resolution, sensitivity, and linearity for Tc-99m, and presents initial images obtained with I-123 HIPDM in humans. Resolution and sensitivity measurements with I-123 are also reported.

## METHODS

A photograph of the prototype instrument is shown in Fig. 1. Both high-resolution and high-efficiency aperture rings have been constructed for SPRINT as shown in Fig. 2; they have slit widths of 3.2 mm and 5.6 mm, respectively. In both, the slit length is 15 mm and the ring radius is 16 cm.

For each aperture ring, line source sensitivity and in-plane resolution in air were measured as a function of radial position using hematocrit tubes 75 mm long, filled with Tc-99m. In addition, on-axis values of sensitivity and resolution were obtained for Tc-99m in air and in a 20.5 cm diam, Plexiglas disk and for I-123 in air. Resolution was determined from central profiles taken through images reconstructed using ART (*8*). Volume-source sensitivity was determined for Tc-99m in cylindrical phantoms 19 cm and 20 cm in diam for

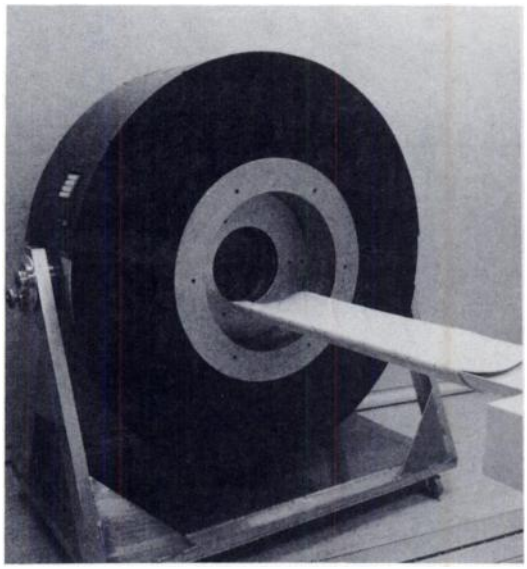

FIG. 1. Photograph of SPRINT. Imaging head pivots about horizontal axis to provide variable angulation of image plane.

FIG. 2. High-resolution and high-efficiency aperture rings. Rings are gear-driven by microprocessor-controlled stepping motor. Optically sensed mark on rim of each ring is used to fix starting position.

each of the aperture rings. Source strength was measured using a dose calibrator.*

Longitudinal resolution was measured on-axis and at a 10-cm radius by shifting a Tc-99m point source in the z direction and recording the total count rate as a function of source position. Longitudinal resolution was also determined for tangential and radial rays at the 10-cm radius.

Response linearity was investigated as a function of pulse-height window setting by imaging a 5-cm thick "pie" phantom with five segments containing Tc-99m in relative concentrations of 0, 1, 2, 4, and 8. The pulse-height windows have a fixed width equal to 20% of their energy settings. Using a line source in air, the energy setting for all detectors is stepped from maximum to minimum under microprocessor control. The setting that gives the peak count rate for each detector is stored. On a second pass the energy setting for each window is stepped upward starting just below the peak count rate setting until a preset decrease from peak count rate is reached for each detector. In this manner the windows can be set to reject varying amounts of Compton-scattered radiation at a known sacrifice in photopeak efficiency. Pie-phantom data were acquired at a peak window setting and at window offsets giving a 10% and 20% decrease from peak count rates for the line source in air. Irregular regions of interest of approximately the same size and shape were manually drawn in each pie segment of the reconstructed images and average counts/pixel were calculated.

Overall image quality has been determined with a Derenzo phantom and by imaging the distribution of HIPDM in three volunteers. The Derenzo phantom is composed of six groups of tracer-filled holes 7 cm long. The hole diam are 6.2, 5.4, 3.5, 3, and 2.5mm. In each case the edge-to-edge hole spacing is 3 hole diam. This phantom was imaged with both aperture rings. Approximately 3 million counts were acquired in each case.

Human volunteers for I-123 HIPDM imaging were solicited by advertising, and informed consent was obtained for the procedure. The HIPDM was labeled with I-123 produced by the $(p,5n)$ reaction and was purity checked by HPLC. A dose of 8 mCi was administered while the volunteer was reading. Ten minutes after injection, data were acquired for a short interval with the slits blocked to determine the amount of high-energy background to be subtracted from the image data. The slice location was 4.9 cm above and oriented $-15°$, with respect to the canthomeatal line. Three 20-min data sets were acquired of this slice using the high-efficiency ring.

Two iterative algorithms are being used for SPRINT image reconstruction: CSIM, a compensated simultaneous updating method described by Snapp (*7*), and ART, a sequential updating algorithm described by Herman (*8*). CSIM is an iterative least-squares type of algorithm in which the error correction is determined experimentally for a given class of problems and then fixed. This avoids the actual least squares calculation in the inner loop of the program. With both ART and

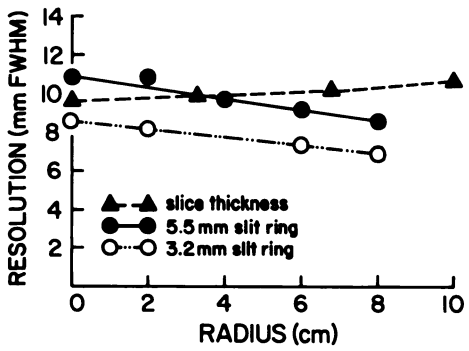


**FIG. 3.** In-plane and cross-plane resolution for 2 aperture rings as function of radial position.

CSIM, the forward projection along each ray is accomplished using a linked list of pixel weights. For each pixel on the diverging finite-width ray, these weights represent the product of detection solid angle and attenuation factor. At present, attenuation is assumed constant in an elliptical region, although any known attenuation map may be used.

Immediately after imaging with SPRINT, images were acquired with a rotating Anger camera for comparison.† One hundred twenty-eight views were acquired using a 15% window width and low-energy, general purpose collimator.‡ Total acquisition time was 32 min. High-energy background was determined by taking a separate data set with 3 mm of lead over the collimator face. Anger-camera images were reconstructed using filtered back-projection. Attenuation correction was accomplished with the Sorenson method (*9*), assuming constant attenuation in an elliptical region, and a Hanning filter with cutoff of 0.7 cycles/cm was used for reconstruction.

## RESULTS

Figure 3 summarizes the in-plane and cross-plane resolution measurements for the two aperture rings. For Tc-99m in air, in-plane resolution varies linearly from 8.5 mm FWHM on-axis to 6.9 mm FWHM at 8 cm off-axis for the high-resolution ring. On-axis resolution drops to 10.4 mm FWHM when the source is placed at the center of the 20.5-cm Plexiglas disk. Measurements for the high-sensitivity ring in air give 10.8 mm and 8.5 mm FWHM on-axis and at 8 cm, respectively. This ring gives an on-axis resolution of 11.1 mm FWHM for I-123. In general, the point-source resolution was degraded 15 to 20% when CSIM was used to reconstruct the images instead of ART. Isolated point images were circularly symmetric with both algorithms even for points at an 8-cm radius.

Slice thickness resolution for Tc-99m at the center and edge of the field of view is respectively 1.0 and 1.05 cm FWHM. These values agree within a millimeter with the collimation design values. FWTM values at the center and edge are 1.75 cm and 1.80 cm, respectively. Tangential and radial rays at 10-cm radius have equal FWHM resolution, but FWTM resolution is 1.5 cm for tangential rays and 1.9 cm for radial rays when the spread functions for opposing detectors are summed.

Table 1 summarizes results of the sensitivity measurements for the two aperture rings. The high-sensitivity ring gives a 66% increase in sensitivity for a line source and a 69% increase for the volume source. Sensitivity drops 10% as the line source is moved from the center of the field of view to a position 8 cm off-axis. The measured sensitivity for an I-123 line source is 9% lower than that for a Tc-99m source. The volume sensitivity of 989

**TABLE 1. SPRINT SENSITIVITY**

| Line sources | Radial source position 0 cm | 2 cm | 4 cm | 6 cm | 8 cm |
|---|---|---|---|---|---|
| H.RES. ring | | | | | |
| Tc-99m (air)* | 434 | 431 | 423 | 410 | 390 |
| Tc-99m (Plexiglas)* | 159 | | | | |
| Tc-99m (Plexiglas)† | 120 | | | | |
| H.SENS. ring | | | | | |
| Tc-99m (air)* | 720 | 715 | 702 | 681 | 647 |
| I-123 (air)* | 652 | | | | |

| Tc-99m volume sources | 19 cm diam | 20 cm diam |
|---|---|---|
| H.RES. RING‡ | 886 | 989 |
| H.SENS. RING‡ | 1466 | 1670 |

* Cpm per μCi/cm. Peak pulse-height window setting.

† Pulse-height window offset 10%.

‡ Cps per μCi/cc uniformly distributed in cylinder at peak pulse-height window setting. A 20% offset in pulse-height window reduces flood count rate by ~ 30%.

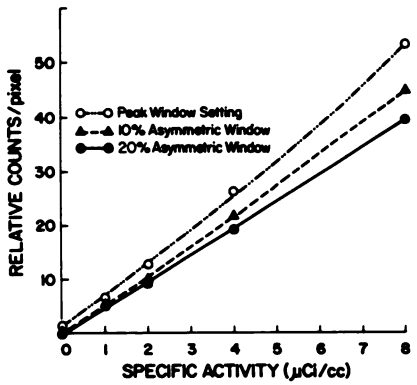


**FIG. 4.** Linearity measurement using Tc-99m. Average count density in each segment of "pie" phantom tomogram (see Fig. 5) was calculated and plotted against known activity of that segment. Results are shown for varying amounts of scatter rejection achieved by shifting pulse-height windows for all detectors to higher energy, as described in text. With 20% window offset, plot is linear, with zero intercept.

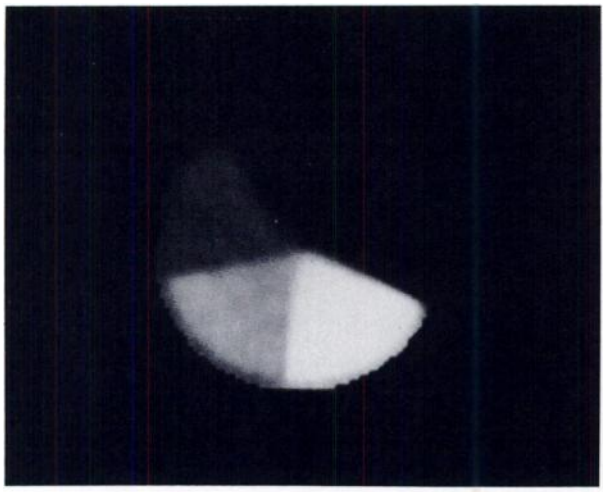

**FIG. 5.** Reconstructed tomogram of pie phantom with 10% window offset. Compensated simultaneous method (CSIM) was used for image reconstruction, and eighth iteration is shown. Relative specific activities of Tc-99m in five segments are 0, 1, 2, 4, and 8.

cps per $\mu$Ci/cc for the 20-cm-diam cylindrical source corresponds closely to the previously published results (*6*) based on a single detector and a symmetric pulse-height window 18% wide. Direct comparison is complicated by the fact that about a third of the detectors have pulse-height resolutions worse than 15% FWHM, and because the method used to set the windows for the entire ring is not equivalent to setting a symmetric 18% wide window on the photopeak.

Results of the linearity measurement are given in Fig. 4. The effects of Compton scattering are clearly shown. For a pulse-height window set for peak count rate, the plot of counts per image element against specific activity of the source is not a straight line and does not go through zero. For a 10% window offset the curve is appreciably straighter and has a zero intercept. With a 20% window offset, the curve is linear and has a zero intercept. Compton scatter in this phantom introduces as much as a 35% increase in the image intensity for the high-activity segment. A reconstructed image of the pie phantom with a 10% window offset is shown in Fig. 5.

CSIM reconstructions of the Derenzo phantom for the two aperture rings are compared in Fig. 6. The improvement in resolution from the center to the edge is readily appreciated for both apertures. All of the 4-mm source elements are resolved with the high-efficiency aperture, whereas the high-resolution aperture resolves the 3.5-mm spots at the center and even a few 2.5-mm spots at the edge of the field of view. These images also show an elliptical response function, with the long axis oriented radially, for source elements toward the edge of the field. As shown in Fig. 6 (right) the ART reconstruction of the high-resolution data is considerably noisier but does not show an elliptical response function.

Figure 7 shows the HIPDM images obtained with SPRINT. The three images are reconstructed from 200k, 400k and 600k counts after background subtraction, and represent 20, 40, and 60 min of acquisition

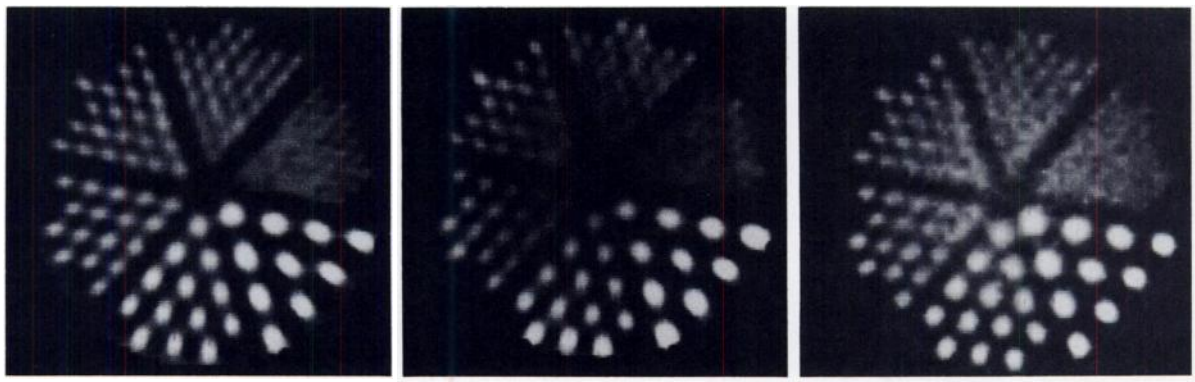

**FIG. 6.** Comparison of Derenzo phantom images obtained with high-resolution aperture ring (left) and high efficiency ring (center). Eight iterations of CSIM were used to obtain these images. Six iteration ART reconstruction of high-resolution data is shown to demonstrate image dependence on algorithm (right). Note increased noise together with absence of elliptical distortion. Images contain 3 million counts and are reconstructed on 64 × 64 matrix.

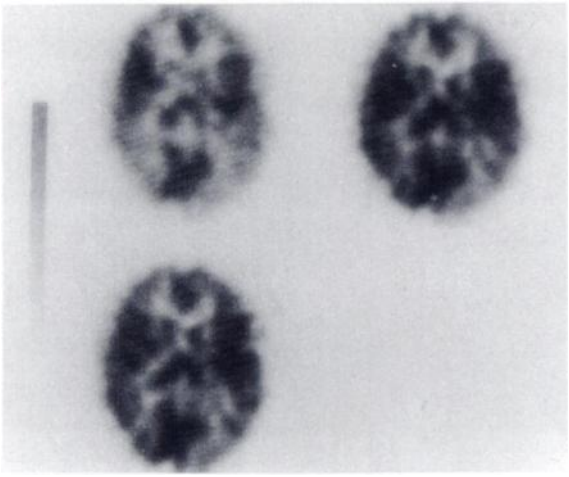

FIG. 7. I-123 HIPDM tomograms of a normal volunteer obtained with SPRINT. Slice is 4.9 cm above and angled approximately −15° to C-M line. Starting at upper left are images containing 200k, 400k and 600k counts representing 20, 40 and 60 min imaging. Final image is somewhat blurred by motion.

time. The raw images were smoothed with an 11-point FIR filter with half-power point at 0.8 cycles/cm. The illustrated slice passes through the head of the caudate nucleus, thalamus and visual cortex. The asymmetry observed near the occipital is possibly related to left-eye amblyopia, which the volunteer exhibited from early childhood.

For comparison, an image obtained with the rotating camera is shown in Fig. 8. The illustrated slice is one pixel (6 mm) thick and contains 90,000 counts. Acquisition time was 32 min. The same general brain structure is shown as in Fig. 7 but with about half the spatial resolution. This resolution loss is primarily a result of the large radius of rotation required to clear the subject's shoulders, as illustrated by the camera images of the Derenzo phantom shown in Fig. 9, which were taken at 15- and 19-cm radius of rotation. Although some redistribution of HIPDM has taken place between the two imaging sessions, images of virtually identical quality were obtained when the order of imaging was reversed for other subjects.

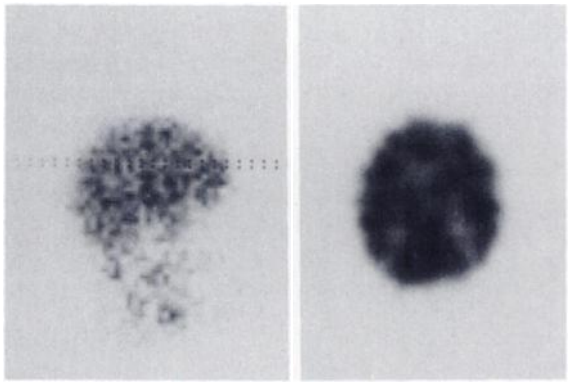

FIG. 8. SPECT tomogram of same volunteer illustrated in Fig. 7. Approximately same slice is illustrated although there is slight change in head angulation. Image is one pixel thick, which corresponds to 6 mm. Actual slice resolution is approximately 15 mm.

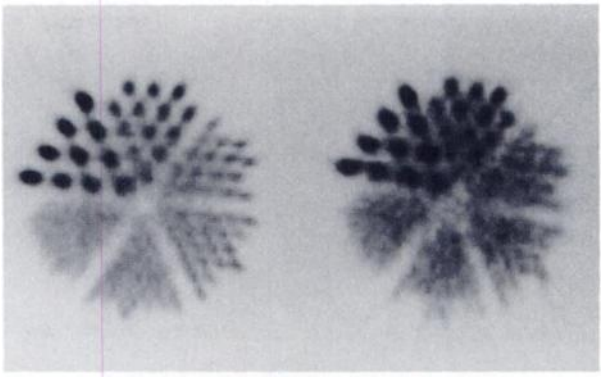

FIG. 9. SPECT tomograms of Derenzo phantom taken with radius of rotation = 15 cm (L) and 19 cm (R).

## DISCUSSION

In-plane resolution for both the high-resolution and high-sensitivity aperture rings appears sufficient to resolve much brain anatomy of interest. The 70% increase in efficiency that is obtained with the high-efficiency ring is probably worth the loss of 2 mm resolution particularly in a single-slice instrument.

The observed 9% difference in sensitivity between Tc-99m and I-123 in air is probably not real, but due to differences in energy window setting or source calibration. Additional measurements will be required to clarify this.

Slice thickness resolution and line-source sensitivity in air are both remarkably uniform from the center to a radius of 8 cm, with resolution varying only 5% and sensitivity dropping only 10%. The fact that tangential and radial rays at the edge of the field of view have equal slice-thickness resolution helps to minimize inconsistency in the data set.

Results obtained with the "pie" phantom show that SPRINT is capable of quantitative imaging. These results also serve to illustrate the difficulties of quantitative imaging in the presence of Compton scatter. The number of Compton-scattered gamma rays detected depends not only upon the pulse-height window setting, but also the spatial distribution of activity in the source. In this case, since there was no activity in slices adjacent to the photopenic segment, this phantom substantially underestimates the amount of scatter that would be present in a clinical situation even with offset pulse-height windows. Unless methods can be found to successfully deconvolve the Compton point-spread function, it is evident that it will be difficult to achieve quantitative accuracy for general source distributions.

Images of the Derenzo phantom obtained with

SPRINT are in general agreement with the measured response function. The elliptical distortion of the peripheral source elements does not arise from differences in source-to-aperture geometry for the radial and tangential rays. In fact, calculation shows the tangential rays to have 10% higher in-plane resolution than the radial rays. Although the point-response function for both algorithms is circularly symmetric down to 25% of maximum, some asymmetry is evident at 10% of maximum for the CSIM algorithm, which probably results in the observed distortion for the Derenzo phantom. Nevertheless, it is surprising that ART and CSIM give such different line-response shapes, and this effect requires further investigation.

Both the single-slice detection efficiency and resolution of SPRINT are double that of the single Anger camera used in this comparison. The Anger camera, however, is capable of much higher performance when equipped with slant-hole (*10,11*) or converging collimators (*12*). The sensitivity, of course, is also proportional to the number of heads. In fact, based on analysis, there should not be major differences in performance between a well-designed ring system and a multicamera system that surrounds the patient, provided both are designed for the same resolution and field of view (*6*).

SPRINT performance may also be compared with another ring system, Headtome II, which uses an ingenious varying pitch collimator (*13*). The in-plane resolution of the two systems is virtually identical, but the slice thickness of Headtome II is 1.8 cm compared with 1.0 cm for SPRINT. The efficiency for a single slice measured with a 20-cm diam phantom containing Tc-99m is 9800 cps/$\mu$Ci/cc compared with 1000 cps/$\mu$Ci/cc for SPRINT. This difference is due to the combination of wider slice thickness, higher detector packing fraction (80% compared with 30%), and smaller detector radius for Headtome II.

The principal advantages of SPRINT are its stationary detector system, mechanical simplicity, and light, inexpensive, and easily changed collimation. Its uniform slice thickness for both radial and tangential rays and the ability to use offset energy windows without introducing spatial distortion contribute to its high-image quality.

Despite the fact that the prototype SPRINT has only a 30% detector packing fraction, it is clearly capable of clinical imaging. Its biggest disadvantage is that it is a single-slice instrument so that if more than two or three slices are required for a given study, the imaging time becomes excessive. Although it would be possible to increase the efficiency by degrading the resolution, it seems preferable to extend the basic design concept to a smaller diam instrument with high detector packing fraction, which samples continuously in the z direction. Such a project is, in fact, under way.

In summary, the basic design goals of the prototype instrument have been met. High-quality, quantifiable tomograms with 1-cm resolution can be achieved with a stationary detector system using slit collimation. The efficiency is high enough to permit clinical brain imaging provided no more than 2 or 3 slices are required.

## FOOTNOTES

* Capintec.
† GE-400AT
‡ GE-Low Energy General Purpose

## ACKNOWLEDGMENT

This work was supported by the National Cancer Institute Grant # R01 CA32846. The authors acknowledge the secretarial assistance of Diane Vecellio in preparation of the manuscript and Tom Mangner for preparation of the I-123 HIPDM.

## REFERENCES

1. WINCHELL HS, HORST WD, BRAUN L, et al: N-isopropyl [$^{123}$I] p-iodoamphetamine: Single-pass brain uptake and washout; binding to brain synaptosomes; and localization in dog and monkey brain. *J Nucl Med* 21:947–952, 1980
2. KUHL DE, BARRIO JR, HUANG S-C, et al: Quantifying local cerebral blood flow by N-isopropyl-p-[$^{123}$I]-iodoamphetamine (IMP) tomography. *J Nucl Med* 23:196–203, 1982
3. HILL TC, HOLMAN BL, LOVETT R, et al: Initial experience with SPECT (single-photon computerized tomography) of the brain using N-isopropyl I-123 p-iodoamphetamine: Concise communication. *J Nucl Med* 23:191–195, 1982
4. KUNG H, TRAMPOSCH K, WICKS R, et al: Synthesis and biodistribution of I-123 HIPDM: A new brain perfusion imaging agent. *J Nucl Med* 23:P22, 1982 (abst)
5. FREY KA, WIELAND DM, BROWN LE, et al: Development of a tomographic myelin scan. Annals of Neurology 10: 214–221, 1981
6. ROGERS WL, CLINTHORNE NH, STAMOS J, et al: SPRINT: A stationary detector single photon ring tomograph for brain imaging. *IEEE Trans Med Im* 1:63–68, 1982
7. SNAPP WP: Reconstruction methods for nuclear emission tomography. Technical report # SEL-TR-144. Systems engineering laboratory. University of Michigan, 1980
8. HERMAN GT, LENT A: Iterative reconstruction algorithms. *Comput Biol Med* 6:273–294, 1976
9. SORENSON JA: Methods for quantifying radioactivity in vivo by external counting measurements. PhD Thesis (University of Wisconsin) 1971
10. POLAK JF, HOLMAN BL, MORETTI J-L, et al: I-123 HIPDM brain imaging with a rotating gamma camera and slant-hole collimator. *J Nucl Med* 25:495–498, 1984
11. ESSER PD, MITNICK RJ, ARLISS J, et al: Angular single photon emission computed tomography (SPECT): An improved method for cranial tomographic imaging. *J Nucl Med* 24:P75, 1983 (abst)
12. JASZCZAK RJ, CHANG LT, MURPHY PH: Single photon emission computed tomography using multislice fan beam collimators. *IEEE Trans Nucl Sci* NS-26:610–616, 1979
13. HIROSE Y, IKEDA Y, HIGASHI Y, et al: A hybrid emission CT—Headtome II. *IEEE Trans Nucl Sci* NS-29:520–523, 1982